

Spread Spectrum Time Domain Reflectometry and Steepest Descent Inversion to Measure Complex Impedance

Samuel R. Kingston¹, Hunter Ellis¹, Mashad U. Saleh¹, Evan J. Benoit¹,
Ayobami Edun², Cynthia M. Furse^{1,3}, Michael A. Scarpulla¹, and Joel B. Harley²

¹Department of Electrical and Computer Engineering
University of Utah, Salt Lake City, UT, 84112, USA
samuel.kingston@utah.edu, hunter.ellis@utah.edu, mashad.saleh@utah.edu, evan.benoit@utah.edu,
cynthia.furse@utah.edu, mike.scarpulla@utah.edu

²Department of Electrical and Computer Engineering
University of Florida, Gainesville, FL, 32611, USA
aedun@ufl.edu, joel.harley@ufl.edu

³LiveWire Innovation, Camarillo, CA, 93012, USA

Abstract — In this paper, we present a method for estimating complex impedances using reflectometry and a modified steepest descent inversion algorithm. We simulate spread spectrum time domain reflectometry (SSTDR), which can measure complex impedances on energized systems for an experimental setup with resistive and capacitive loads. A parametric function, which includes both a misfit function and stabilizer function, is created. The misfit function is a least squares estimate of how close the model data matches observed data. The stabilizer function prevents the steepest descent algorithm from becoming unstable and diverging. Steepest descent iteratively identifies the model parameters that minimize the parametric function. We validate the algorithm by correctly identifying the model parameters (capacitance and resistance) associated with simulated SSTDR data, with added 3 dB white Gaussian noise. With the stabilizer function, the steepest descent algorithm estimates of the model parameters are bounded within a specified range. The errors for capacitance (220pF to 820pF) and resistance (50 Ω to 270 Ω) are < 10%, corresponding to a complex impedance magnitude $\left| R + \frac{1}{j\omega C} \right|$ of 53 Ω to 510 Ω .

I. INTRODUCTION

Complex impedance measurements are used in a variety of applications, such as antenna design [1], precision agriculture [2], and estimates of photovoltaic (PV) aging [3]. For antenna design, complex impedance is measured to ensure a good match between the source transmission line and the antenna [4]. For precision agriculture, complex impedance is used as a measure of the moisture content in the soil. In PV systems complex

impedance measurements ensure minimal impedance mismatch between the PV panels and charge controllers, for efficient power throughput [5] and the integrity of panels and system [4].

Complex impedance is commonly measured with an inductance-capacitance-resistance (LCR) meter or a vector network analyzer (VNA) [6]–[8]. An LCR meter transmits a small AC voltage signal for a range of frequencies and calculates the complex impedance from the ratio of applied voltage to measured current through the device under test (DUT) [9]. A VNA is similar in that it transmits a small AC voltage and varies frequency, but it calculates the reflection and transmission coefficients at the DUT. From these coefficients and knowledge of the transmission line impedance, the complex impedance is calculated [10].

One of the disadvantages of using an LCR meter or a VNA is that they require the DUT to be disconnected and generally de-energized [9], [10]. PV health monitoring [11] is one example where the system cannot be easily de-energized [12]. In this paper, we propose a new method of measuring complex impedance on energized systems using spread spectrum time domain reflectometry (SSTDR) [13] in conjunction with a steepest descent inversion algorithm.

Reflectometry has been used for detecting and locating electrical faults in transmission lines, aircraft cabling, and PV systems [14], [15]. SSTDR can be used to locate open and short circuit faults on energized systems [13], however there is limited research on using SSTDR to measure complex impedance. In [16], [17] SSTDR is used to measure the impedance of a capacitive load at the end of a transmission line. These methods can

be adapted to measure inductance, but incorporating resistance for a full complex impedance would significantly increase the complexity of the algorithms. In [16], a dictionary matching approach is implemented. Although effective, this method can be computationally expensive. In [17], a curve fitting approach to identify the shape of the signal is used. This is simple and suitable for loads that are strictly capacitive or inductive, but more complex loads cannot be evaluated with this particular algorithm. In [18], SSTDR was used to evaluate single loads (resistor, capacitor, inductor, PV panel) through visual inspection of the time domain SSTDR response. This paper introduces an inverse method based on steepest descent to measure complex impedance(s) (capacitance and resistance simultaneously), that is both computationally efficient and accurate.

Inversion algorithms are used in radar, acoustics, geophysics, computer vision, and other fields [19]–[21]. The inverse problem consists of extracting useful information from experimental/observed data [21]. Model parameters, which are often found iteratively, describe the observed data and are used to generate predicted data that fit best with the observed data. Steepest descent algorithms are relatively simple, accurate, and computationally efficient [21]. Although steepest descent inversion has a history in geophysics and other fields [22], it has not yet been applied to SSTDR. This paper describes a computationally efficient and accurate method to measure complex impedance using SSTDR and steepest descent.

This paper combines the ability of SSTDR to measure in live systems with an efficient steepest descent inversion algorithm to determine complex impedances from SSTDR responses. We validate this approach by simulating an SSTDR signature with a known complex load impedance (a series connected capacitor and resistor) and add white Gaussian noise to represent experimental data. We demonstrate that our new algorithm accurately estimates impedance from these noisy SSTDR signals. Algorithms used in previous work [16] were able to evaluate capacitance from 278 pF to 409 pF with less than 10% error, and we will show similar results, as well. These algorithms used the shape of the time domain signal for capacitance measurement. However, for complex impedances (including resistance), this time domain analysis is more complicated. In this paper, we will use a steepest descent algorithm in the frequency domain, thus enabling efficient measurement of both capacitance and resistance simultaneously.

II. METHODOLOGY

To measure the complex impedance, we solve an inverse problem using steepest descent [21], [23]. First, we define the inverse problem in terms of the observed data space and the model space. Next, we define the parametric function, which is the function we seek to

minimize with a steepest descent algorithm. The parametric function is a combination of the misfit function and a stabilizer function [21]. Through sampling the misfit function, we show that the model space has a unique solution within the bounds of the sampled model space. Finally, we show the steepest descent algorithm using regularization to measure complex impedance. The main purpose of this paper is to demonstrate the methodology. Therefore, we use a relatively simple example of measuring series-connected capacitance and resistance, where the test signal is simulated SSTDR data with added white Gaussian noise to be more representative of experimental data.

A. Setting up the inverse problem

The inverse problem is the solution to the function:

$$\mathbf{d} = A(\mathbf{m}), \quad (1)$$

where data \mathbf{d} is a $4,096 \times 1$ frequency dependent vector in the observed SSTDR response data space associated with an unknown complex impedance. We have modeled this unknown impedance as a resistor (R) and capacitor (C) connected in series. From (1), \mathbf{m} is a 2×1 vector of the model parameters (R and C). The model space $A(\mathbf{m})$ is the function acting on the model parameters \mathbf{m} to get \mathbf{d} .

The observed data \mathbf{d} and model data $A(\mathbf{m})$ are SSTDR signatures (converted to the frequency domain) resulting after transmitting an incident 12MHz SSTDR signal, $X(\omega)$, through 27.5 m of 10 AWG PV cable (with parameters given in [24]), as shown in Fig. 1. The 27.5 m cable was long enough to separate reflections from the load from those between the SSTDR instrument and the transmission line. We include in the simulation the complex impedance of the SSTDR, $Z_{SSTDR}(\omega)$, the incident simulated signature, $X(\omega)$, the transmission line characteristic impedance, Z_0 , the load, $R + \frac{1}{j\omega C}$, the reflection coefficient $\Gamma(\omega)$ between Z_0 and the capacitor-resistor load, and the transmission coefficient, $T(\omega)$, between Z_{SSTDR} and Z_0 . The transmission line characteristics used to model the characteristic impedance, Z_0 , are defined in [17] using a twin-lead transmission line model for the PV cable.

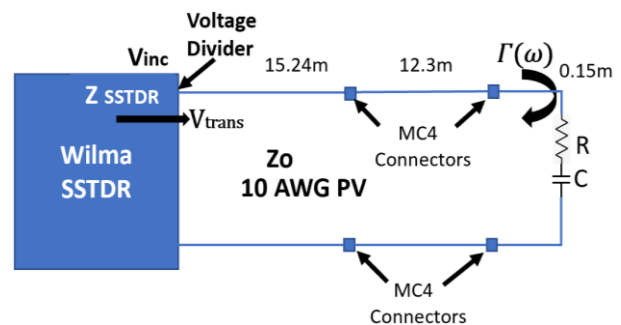


Fig. 1. Experimental setup for measuring SSTDR responses from a capacitive-resistive load.

The observed data, \mathbf{d} , and the model data in $\mathbf{A}(\mathbf{m})$ are simulated by the frequency response of a *sinc*-like incident signal, $X(\omega)$, multiplied by the reflection coefficient, $\Gamma(\omega)$, and transmission coefficient, $T(\omega)$, as:

$$\mathbf{d}_{m=\{R,C\}} \text{ and } \mathbf{A}(\mathbf{m})_{m=\{R,C\}} = X(\omega)\Gamma(\omega)T(\omega). \quad (2)$$

From [16] $X(\omega)$ is calculated as the Fourier transform of the expected value of the autocorrelation between the incident and reflected SSTDR signals. The reflection coefficient $\Gamma(\omega)$ is calculated as:

$$\Gamma(\omega)_{m=\{R,C\}} = \frac{\left(R + \frac{1}{j\omega C}\right) - Z_o}{\left(R + \frac{1}{j\omega C}\right) + Z_o}, \quad (3)$$

where R and C represent the resistance and capacitance of the load impedance. The transmission coefficient, $T(\omega)$, is calculated as a voltage divider between the impedance of the SSTDR, $Z_{SSTDR}(\omega)$, and the transmission line, Z_o , as:

$$T(\omega) = \frac{Z_{SSTDR}(\omega)}{Z_o + Z_{SSTDR}(\omega)}, \quad (4)$$

The time domain SSTDR response from (2) for the system shown in Fig. 1 is time-gated [17] to include only the part of the signal where the reflection from the load is seen, and converted to the frequency domain. The propagation through the transmission line is assumed to be ideal (lossless with constant velocity of propagation). Loss and dispersion could be accounted for by adding an additional transfer function with these effects to (2).

For our purpose of testing the algorithm, \mathbf{d} is a column vector of simulated SSTDR data for a known R and C value, with 3 dB added white Gaussian noise. For a validation test, the known R and C values were chosen to be 200 Ω and 300 pF, respectively. The rows in \mathbf{d} show the complex energy for each frequency in the bandwidth of the SSTDR signature, \mathbf{d} . The SSTDR response for a 12 MHz signal covers the frequency band from -24 MHz to +24 MHz, with a frequency spacing of 11.719 kHz, with the highest energy centered at 12MHz [16] and 4096 frequency samples (rows) from -24MHz to +24MHz.

B. Parametric function: Misfit and regularization

We solve for the model parameters of the simulated noisy data, \mathbf{d} , through a least squares approximation of the parametric function, which is a combination of the misfit function and regularization, similar to [21]. The misfit function is a measure of closeness between the SSTDR responses in the model space, $\mathbf{A}(\mathbf{m})$, and the simulated noisy SSTDR response, \mathbf{d} . The misfit function, $\phi_d(\mathbf{m})$, also termed the residual, is calculated for each k^{th} iteration of the steepest descent algorithm as:

$$\phi_d(\mathbf{m}) = \|\mathbf{A}(\mathbf{m}_k) - \mathbf{d}\|^2. \quad (5)$$

The least squares minimum best estimate of the model parameters is found when:

$$\phi_d(\mathbf{m}) \leq \eta^2, \quad (6)$$

where η^2 is the noise energy level of the simulated noisy data, \mathbf{d} . In this example, the observed (measured) data is simulated with added white noise, so that the SNR = 3 dB.

To establish that there is a unique solution for (1) within the bounds of interest for a known load ($C = 300$ pF, $R = 200 \Omega$), we sampled the parameter space of $\mathbf{A}(\mathbf{m})$ to get a matrix, \mathbf{A} , where each column, \mathbf{a}_i , in \mathbf{A} is a simulated SSTDR response from a unique R and C value. We chose the sampled parameter space to be 200 capacitors, logarithmically spaced between 1 pF and 1,000 pF and 80 resistors, linearly spaced between 50 Ω and 500 Ω . It is expected that the unknown RC combination will lie somewhere in this range. \mathbf{A} has 16,000 columns (200 capacitors x 80 resistors) and 4,096 rows for the complex energy values of each frequency in the SSTDR signature.

The misfit (5) for every SSTDR signature in \mathbf{A} is plotted in Fig. 3 as a function of the two model parameters, R (horizontal axis) and C (vertical axis), for one test scenario where the observed data, \mathbf{d} , was simulated using a load $C=300\text{pF}$ and $R=200\Omega$. The color shows the misfit for the respective model space signatures. Dark blue represents the minimum of the misfit function, where the simulated model data, $\mathbf{A}(\mathbf{m})$, closely matches the observed data, \mathbf{d} .

Regularization was used to make the parametric function more robust and reduce sensitivity to small variations in the data [21]. This enables the steepest descent algorithm to keep model parameters within a specified range (in our case the range of \mathbf{A}) and enables it to identify the correct model parameters. The regularization was calculated using the stabilization function:

$$\phi_m(\mathbf{m}) = \alpha \|\mathbf{m} - \mathbf{m}_{\text{apr}}\|^2, \quad (7)$$

where α is the estimated regularization factor, described in more detail in the next section. The \mathbf{m} in (7) is the vector of model parameters (R and C), and \mathbf{m}_{apr} is the median $C=500\text{pF}$ and median $R=250\Omega$ in the sampled space of \mathbf{A} . The medians of both the R and C were chosen to keep the steepest descent estimates within the sampled space.

The algorithm requires an estimated range (max and min) of the model parameters, and there is a tradeoff in robustness vs. efficiency of the algorithm. The broader the range, the more likely the algorithm is to converge to the correct values, but it could take many more iterations. If the range is narrower, the algorithm can converge with fewer iterations, but if the model parameters are outside the range, the correct values would be missed.

Combining the misfit function $\phi_d(\mathbf{m})$ and stabilization function $\phi_m(\mathbf{m})$, the parametric function becomes:

$$\mathbf{P}^\alpha(\mathbf{m}, \mathbf{d}) = \phi_d(\mathbf{m}) + \phi_m(\mathbf{m}). \quad (8)$$

We identify the correct model parameters by using steepest descent to iteratively find the minimum solution to (8).

C. Applying a steepest descent algorithm to measure capacitance and resistance

To find the minimum of the parametric function (8), we apply a modified steepest descent algorithm [21]. Steepest descent starts with an initial guess of the model parameters and iteratively identifies the parameters within the model space, $A(\mathbf{m})$, that are closest to the model parameters in \mathbf{d} . The steepest descent algorithm has three steps: Step 1, make an initial guess of the model parameters, \mathbf{m}_0 . Step 2, from the parameters around this guess, identify the direction within the model space, $A(\mathbf{m})$, which results in the greatest slope. Step 3 is to move in this direction to find the next model parameters within $A(\mathbf{m})$. Step 4 is to repeat steps 2 and 3 until the model data $A(\mathbf{m})$ from the estimated model is within the noise level of the observed data, \mathbf{d} .

For our case, the initial model parameter guess is an RC combination within the range of the model space, $A(\mathbf{m})$. Next, we follow the steepest descent method [21] and define the change of the model parameters for each iteration as:

$$\delta\mathbf{m} = -k^\alpha \mathbf{l}^\alpha(\mathbf{m}), \quad (9)$$

where the length of a step in the iteration process, k^α , is a positive real number. The vector $\mathbf{l}^\alpha(\mathbf{m})$ is a column vector defining the direction of steepest descent of the parametric function (8), which is calculated using the Fréchet derivative [21] of C and R. Normalization is applied to $\mathbf{l}^\alpha(\mathbf{m})$ to make the step size in the direction of both R and C the same order of magnitude. Specifically, $\mathbf{l}^\alpha(\mathbf{m})$ is multiplied by the inverse of the parameter with smaller magnitude, which is C. The steepest descent method is an iterative process of finding each \mathbf{m} according to:

$$\mathbf{m}_{n+1} = \mathbf{m}_n + \delta\mathbf{m} = \mathbf{m}_n - k^\alpha \mathbf{l}^\alpha(\mathbf{m}), \quad (10)$$

where the step size k_n^α is defined by the line search method [16] as:

$$k_n^\alpha = \frac{\|\mathbf{l}^\alpha(\mathbf{m})\|^2}{\|\mathbf{F}\mathbf{l}^\alpha(\mathbf{m})\|^2 + \|\mathbf{l}^\alpha(\mathbf{m})\|^2}, \quad (11)$$

where $\mathbf{F}\mathbf{l}^\alpha(\mathbf{m})$ is the Fréchet derivative of the current model parameters, \mathbf{m}_n , multiplied by the direction of steepest descent, $\mathbf{l}^\alpha(\mathbf{m})$, and α is the regularization factor used to hold \mathbf{m}_n within the bounds of the sampled space.

In the iteration process, the regularization factor, α , starts with a value of zero. The value after the first iteration is determined so that the stabilization function, $\phi_m(\mathbf{m})$, matches \mathbf{m}_1 as a ratio to balance the misfit and the stabilizer functions [21] as:

$$\alpha_1 = \frac{\|A(\mathbf{m}_1) - \mathbf{d}\|^2}{\|\mathbf{m}_1 - \mathbf{m}_{apr}\|^2}. \quad (12)$$

Then for each k^{th} iteration α_k is updated according to:

$$\alpha_k = \alpha_1 q^{k-1}, \quad (13)$$

where k is the steepest descent loop iteration, and q is a normalizing constant chosen to be 0.5. The iterative

process is terminated when the misfit, $\phi_d(\mathbf{m})$, reaches the given noise level, η^2 , of the observed data.

In this section, we have shown that there is a unique solution of the inverse problem in (1) within the bounds of the sampled parameter space for measuring complex impedance. This is shown in Fig. 3 for one test case. A steepest descent algorithm with regularization was used to iteratively identify the complex impedance associated with SSTDR signals. However, the algorithm may experience instability when the residual for the current model parameters is close to the residual for neighboring model parameters. As a result, the step size, k_n^α , will sometimes overshoot out of the bounds of interest [25]. This can happen when the residuals of differing model parameters are close, which happens if the impedance of the loads are nearly the same. For example, a large capacitance ($Z = \frac{1}{j\omega C}$) appears nearly like a short circuit ($Z = 0 \Omega$) [16]. How close these are depends on the frequency, ω , (for higher ω , the impedance of a capacitor is closer to a short circuit). Similar effects are seen for loads that combine capacitance, resistance, and inductance.

To solve the overshoot issue, the algorithm checks if the new estimated model parameters for each iteration are within range. If not, the algorithm implements a random restart [25] by choosing a random RC combination within the bounds of interest. Then the algorithm continues normally. Figure 2 shows a flow chart summarizing the steps to determine the complex impedance.

D. Steepest descent for measuring complex impedance

In this section, we evaluate how effective the steepest descent algorithm is in measuring the complex impedance associated with an observed SSTDR signature. The model parameters (R and C) are found such that the residual of the parametric function (8) is $< 1\%$ above the noise level of the simulated noisy SSTDR data. We tested the algorithm for 25 standard resistor values ranging from 51 Ω to $\sim 510 \Omega$, where $R=[51, 56, 62, 68, 75, 82, 91, 100, 110, 120, 130, 150, 160, 180, 200, 220, 240, 270, 300, 330, 360, 390, 430, 470, 510] \Omega$ and 19 standard capacitor values ranging from 1 pF to 1,000 pF, where $C=[5, 10, 15, 22, 33, 47, 100, 120, 130, 150, 180, 220, 330, 470, 560, 680, 750, 820, 1,000] \text{pF}$.

The ranges for R and C were chosen so that the associated SSTDR responses would be distinguishable from one another. and so they would not appear as an open or a short [16]. The resistors and capacitors were connected in series, giving 475 (25x19) total RC combinations. The range for where a $f=12 \text{ MHz}$ SSTDR signature has highest energy from the load $\left\| R + \frac{1}{j2\pi f C} \right\|$ is from 51.7 to 2,699 Ω .

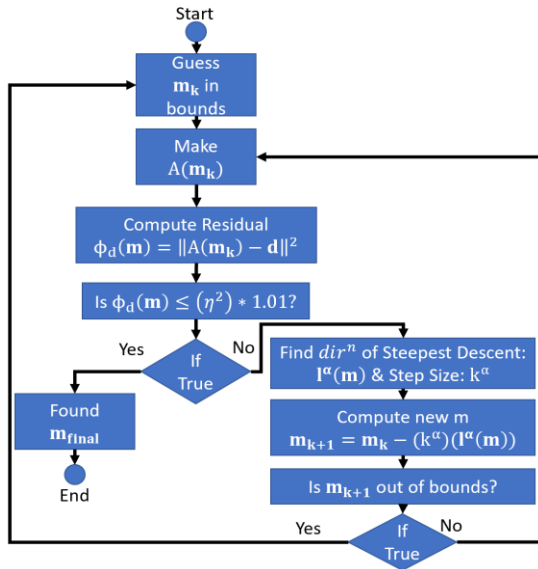


Fig. 2. Flow chart for steepest descent algorithm to measure complex impedance.

Our metric of success is when both model parameters (R and C) are measured with percent error $\leq 10.5\%$. Of the 475 different load combinations tested, 200 were successful (42%). Best results (success $> 92\%$) were found when $51 \Omega < R < 270 \Omega$ and, simultaneously, $220 \text{ pF} < C < 820 \text{ pF}$. This successful range corresponds to $53 \Omega < \left\| R + \frac{1}{j\omega C} \right\| < 276 \Omega$. For impedances tested outside of this range, the probability of success was 25%.

Table 1 shows the results for 10 of the 475 RC combinations tested. The results include the known (true) values, the estimated values, the number of iterations to get the final estimations, and the % error for both the R and C estimates. Rows 3 through 9 show RC combinations within the defined range of success where the error is $< 10.5\%$. Rows 1, 2, and 10 show results for combinations outside this range, with higher % error. Some tests (e.g., row 1) still provide good estimates, however, success is not ensured. In some cases (e.g., row 2) the algorithm takes the maximum number of iterations (10,000) and still does not converge well.

Table 1: Results of modified steepest descent algorithm

True R (Ω)	True C (pF)	Est. R (Ω)	Est. C (pF)	# Iter.	Error % R	Error % C
51	100	54.4	99	35	6.69	0.07
51	120	202.6	21.8	10,000	297	81.8
51	220	53.7	218	63	5.45	0.87
56	470	55.8	461	5	0.42	2.00
62	560	63.3	557	127	2.12	0.56
120	470	119.9	458	11	0.09	2.62
200	330	204.8	342	21	2.38	3.59
220	820	223.3	795	42	1.48	3.05
270	220	262.6	205	60	2.76	6.82
330	750	330.8	581	185	0.26	22.6

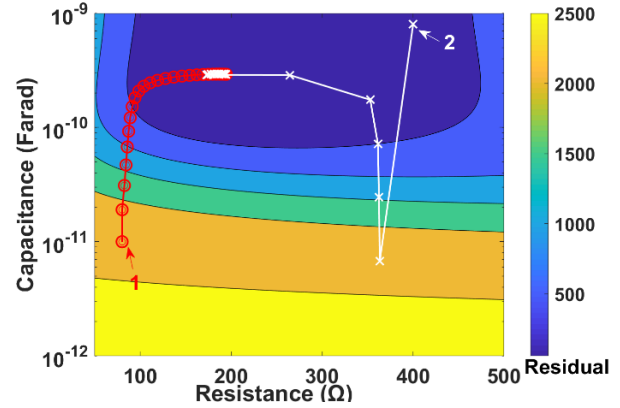


Fig. 3. Misfit as a function of $A(\mathbf{m})$ parameters resistance and capacitance for two separate initial guesses.

The initial guess matters, as shown from the two different convergent paths to the correct estimate, shown in Fig. 3. Path 1 starts with the initial guessed model parameters, $C=10\text{pF}$ and $R=80 \Omega$, and follows the red circles showing the residuals for each iteration of the steepest descent algorithm. The initial guess has a residual $\sim 2,000$, as indicated by the color. Through successive iterations, the residual approaches zero, where the simulated model data, $A(\mathbf{m})$, matches the observed data, \mathbf{d} .

Path 2 in Fig. 3 illustrates the need for a random restart modification. It starts with the initial guessed model parameters, $C=800\text{pF}$ and $R=400 \Omega$. Note that the resistance value is outside the range of success. Also, the residuals of both the initial model parameters and its neighboring values are close, which causes the step size to overshoot the boundaries of allowable guesses. The algorithm would normally guess a set of model parameters within the bounds of interest (often getting stuck there), but because of the random reset, it jumps to some different random parameters within the range. From the new estimate, path 2 can converge to the minimum and identify the correct model parameters. The final estimated parameters for both paths 1 and 2 are $R=199 \Omega$ and $C=299 \text{ pF}$ for the correct model parameters in \mathbf{d} that are 200Ω and 300 pF . Thus, the error for both C and R is $< 1\%$. The number of iterations is dependent on the initial guessed model parameters and the observed data model parameters.

In Fig. 4, we show the convergence of the residuals at each iteration for the two initial guess paths illustrated in Fig. 3. With each progressive iteration in the steepest descent algorithm, the model data is closer to the observed data, and the residual converges to 55, which is below the noise energy level ($=59$) of the simulated noisy data, \mathbf{d} . For path 2, marked with black Xs, the first guessed parameter has a relatively low residual. It then jumps to a higher residual because of the new random guess and progresses to lower residuals until it reaches

a value within the noise level. From Figs. 3 and 4, we have shown an example where the steepest descent can correctly identify the model parameters of noisy simulated SSTDR data.

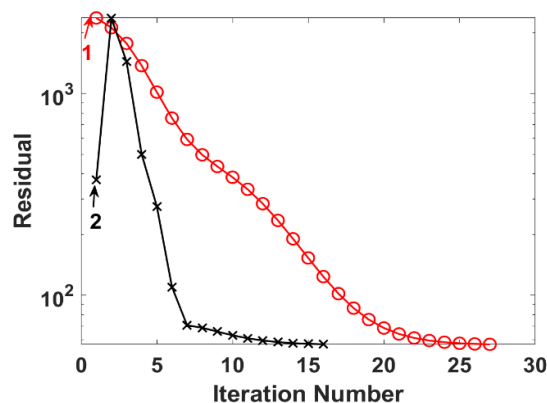


Fig. 4. Convergence of the residual for two different initial guesses. Guess 1 ($C=10\text{pF}$, $R=80\ \Omega$) as red circles and guess 2 ($C=800\text{pF}$ and $R=400\ \Omega$).

E. Steepest descent algorithm complexity

In this section, we discuss the computational complexity of the algorithm and compare it to a similar algorithm. We will estimate complexity by the number of multiplications required per iteration, and the average number of iterations.

For each iteration, the steepest descent algorithm for these examples took 180,256 multiplications. This scales linearly with the number of data points (4,096) in the frequency response. The steps in this algorithm with the largest number of multiplications were calculating the Fréchet derivative (90,130 multiplications) and producing $A(\mathbf{m}_k)$ (20,480 multiplications). The number of iterations depends on the initial guess and model parameters, as described in previous sections. We will use an estimate for the average number of iterations ($N\sim 88$), which was found using the 10% trimmed mean from the tests (e.g., in Table 1) that were within the range of success for both C and R. We used a trimmed mean to remove both the 10% highest and 10% lowest outliers. Note that the mode of the number of iterations was 10, and the median was 46.

From this, when measuring a complex RC impedance within the range of success, the typical number of multiplications is 15.8 million (180,256 multiplications \times 88 iterations). For comparison, in [16], an SSTDR response dictionary was used to measure a single parameter (capacitance). If the dictionary were expanded to include combinations of 1,000 C and 1,000 R values, it would contain 1 million (1,000 \times 1,000) SSTDR responses (each with 4,096 data points). Measuring both C and R would take ~ 12.3 billion multiplications (4096 \times 3 \times 1,000,000), which is significantly greater than for the steepest descent algorithm.

III. CONCLUSION

Using a simple example with a series connected resistor and capacitor, SSTDR and a modified steepest descent algorithm was shown to be an accurate and computationally efficient solution to measure complex impedance. The significance of using SSTDR is that impedances could be measured on energized systems. For a range of RC combination loads where the associated SSTDR response does not appear as an open circuit or short circuit response [16], we were able to measure their impedances with $< 10.5\%$ error. The successful estimations for R and C ranged from $50\ \Omega$ to $270\ \Omega$ and from $220\ \text{pF}$ to $820\ \text{pF}$, respectively. This corresponds to complex impedance magnitude $53\ \Omega < \left| R + \frac{1}{j\omega C} \right| < 276\ \Omega$.

Some of the computational challenges of the algorithm are discussed next. One challenge is that a single load parameter (R or C) can dominate the control of the SSTDR response shape, which can affect the ability to measure the other parameter. For example, the SSTDR response for an RC combination will resemble an open-circuit response if $C=1\ \text{pF}$ (making the overall impedance large) regardless of what the resistor value is. Another challenge is that the computational complexity is dependent on the initial guess and the number of random restarts required. If the algorithm starts with a poor guess, this will increase the complexity. This idea is illustrated in Figs. 3 and 4, where path 2 takes more iterations to converge than path 1.

ACKNOWLEDGMENTS

This material is based upon work supported by the U.S. Department of Energy's office of Energy Efficiency and Renewable Energy (EERE) under Solar Energy Technologies Office (SETO) agreement number DE-EE0008169 in collaboration with Livewire Innovation and the National Renewable Energy Laboratory. It is also based on ideas and concepts discussed with Dr. Zhdanov, a faculty member of the University of Utah.

DISCLOSURE

Dr. Furse is a co-founder of LiveWire Innovation, Inc. which is commercializing SSTDR technology, and therefore has a financial conflict of interest with this company.

REFERENCES

- [1] P. V. Nikitin, K. V. S. Rao, R. Martinez, and S. F. Lam, "Sensitivity and impedance measurements of UHF RFID chips," *IEEE Trans. Microw. Theory Tech.*, vol. 57, no. 5, pp. 1297-1302, 2009.
- [2] D. L. Corwin and S. M. Lesch, "Apparent soil electrical conductivity measurements in agriculture," *Comput. Electron. Agric.*, vol. 46, no. 1-3, pp. 11-43, Mar. 2005.

- [3] S. P. Bharadwaj, A. E. Ginart, I. N. Ali, P. W. Kalgren, J. R. Celaya, and S. D. Poll, "Solar cells aging estimation based on impedance characterization," *Aerospace Conference*, pp. 1-9, Mar. 2011.
- [4] W. Stutzman and G. Thiele, *Antenna Theory and Design*. Wiley Global Education, 2012.
- [5] V. Schlosser and A. Ghitas, "Measurement of silicon solar cells AC parameters," *ARSEC*, 2006.
- [6] P. A. Cotfas, D. T. Cotfas, P. N. Borza, D. Sera, and R. Teodorescu, "Solar cell capacitance determination based on an RLC resonant circuit," *Energies*, vol. 11, no. 3, Art. no. 3, Mar. 2018.
- [7] R. A. Kumar, M. S. Suresh, and J. Nagaraju, "Facility to measure solar cell ac parameters using an impedance spectroscopy technique," *Rev. Sci. Instrum.*, vol. 72, no. 8, pp. 3422-3426, July 2001.
- [8] D. Rytting, "ARFTG 50 year network analyzer history," in *2008 71st ARFTG Microwave Measurement Conference*, pp. 1-8, 2008.
- [9] IET Labs, Inc., "Precision LCR Meter User and Service Manual," *IET Labs*, 2014.
- [10] Anritsu, "Series 37XXXC Vector Network Analyzer Operations Manual," *Anritsu*, 2004.
- [11] M. N. Akram and S. Lotfifard, "Modeling and health monitoring of DC side of photovoltaic array," *IEEE Trans. Sustain. Energy*, vol. 6, no. 4, pp. 1245-1253, 2015.
- [12] J. Haney and A. Burstein, "PV system operations and maintenance fundamentals," *Next Phase Solar, Inc.*, Aug. 2013.
- [13] P. Smith, C. Furse, and J. Gunther, "Analysis of spread spectrum time domain reflectometry for wire fault location," *IEEE Sens. J.*, vol. 5, no. 6, pp. 1469-1478, Dec. 2005.
- [14] C. M. Furse, M. Kafal, R. Razzaghi, and Y. Shin, "Fault diagnosis for electrical systems and power networks: A review," *IEEE Sens. J.*, pp. 1-1, 2020.
- [15] H. Boudjefdjouf, H. R. E. H. Bouchekara, R. Mehasni, M. K. Smail, A. Orlandi, and F. de Paulis, "Wire fault diagnosis using time-domain reflectometry and backtracking search optimization algorithm," in *31st International Review of Progress in ACES*, pp. 1-2, 2015.
- [16] S. R. Kingston, N. K. T. Jayakumar, M. U. Saleh, E. J. Benoit, A. S. Edun, R. Sun, C. Furse, M. Scarpulla, and J. B. Harley, "Measurement of capacitance using spread spectrum time domain reflectometry (SSTDTR) and dictionary matching," *IEEE Sens. J.*, pp. 1-1, 2020.
- [17] N. K. T. Jayakumar, E. J. Benoit, S. R. Kingston, M. U. Saleh, M. Scarpulla, J. B. Harley, and C. Furse, "Post-processing for improved accuracy and resolution of spread spectrum time domain reflectometry (SSTDTR)," *IEEE Sens. Lett.*, vol. 2, no. 3, 2019.
- [18] C. Furse, N. K. T. Jayakumar, E. J. Benoit, M. U. Saleh, J. LaCombe, M. Scarpulla, J. B. Harley, S. R. Kingston, B. Waddoups, and C. Deline, "Spread spectrum time domain reflectometry for complex impedances: Application to PV arrays," *IEEE AUTOTESTCON*, pp. 1-4, 2018.
- [19] F. Cohen-Tenoudji, B. R. Tittmann, and G. Quentin, "Technique for the inversion of backscattered elastic wave data to extract the geometrical parameters of defects with varying shape," *Appl. Phys. Lett.*, vol. 41, no. 6, pp. 574-576, Sep. 1982.
- [20] M. S. Zhdanov, S. Fang, and G. Hursán, "Electromagnetic inversion using quasi-linear approximation," *GEOPHYSICS*, vol. 65, no. 5, pp. 1501-1513, Sep. 2000.
- [21] *Inverse Theory and Applications in Geophysics*. 2nd ed., Elsevier, 2015.
- [22] M. El-Shenawee, C. Rappaport, D. Jiang, and W. Melsei, "Electromagnetics computations using the MPI parallel implementation of the steepest descent fast multipole method (SDFMM)," *Applied Computational Electromagnetics Society*, vol. 17, no. 2, 2002.
- [23] A. A. Goldstein, "On steepest descent," *J. Soc. Ind. Appl. Math. Ser. Control*, vol. 3, no. 1, pp. 147-151, 1965.
- [24] M. U. Saleh, C. Deline, S. R. Kingston, N. K. T. Jayakumar, E. J. Benoit, J. B. Harley, C. Furse, and M. Scarpulla, "Detection and localization of disconnections in PV strings using spread-spectrum time-domain reflectometry," *IEEE J. Photovolt.*, vol. 10, no. 1, pp. 236-242, 2020.
- [25] R. Jacobs, "Increased rates of convergence through learning rate adaptation," *Neural Netw.*, vol. 1, pp. 295-307, 1988.



Samuel R. Kingston was born in Salt Lake City, Utah, USA in 1991. He received the A.S. degree in Business from Salt Lake Community College, Salt Lake City, in 2011. He received a B.S. degree in Electrical & Computer Engineering from the University of Utah, Salt Lake City, UT, in 2016 and is currently working on a Ph.D. from the University of Utah, Salt Lake City, UT.

From 2017 to current, he has been a Research Assistant with the University of Utah lab working in the algorithms group. He has been working with spread spectrum time domain reflectometry (SSTDTR) in being able to detect, localize, and characterize faults within solar panel system. To date, he has written two conference papers and two journal papers for nondestructive health

monitoring. He is currently working on several other journal papers as well, where each one will be a building block in achieving the overall research team goal. His research interests are in signal processing used for health monitoring, renewable energy alternatives, and creating successful startups from conceptual ideas. In 2016, his senior project team received an award for Best Clinic Project where he worked with L3 Communications to develop a way to detect low probability of intercept (LPI) RADAR signals.



Hunter D. Ellis was born in Murray, Utah, UT, USA, in 1997. He is a current M.S. and B.S. student in Electrical Engineering at the University of Utah. He has been a Research Assistant with the University of Utah since 2018. His research interests include Spread Spectrum Time Domain Reflectometry, Photovoltaic, statistical signal processing, semiconductor physics, numerical simulation methods, adaptive filters, and antennas.



Mashad Uddin Saleh (S'17-) received the B.Sc. Engineering degree in Electrical and Electronics Engineering from Bangladesh University of Engineering and Technology, Dhaka, Bangladesh in 2013. He received the M.S. degree in Electrical Engineering from Michigan Technological University, Houghton, MI, USA in 2016. He is currently working towards the Ph.D. degree in Electrical Engineering at the University of Utah, Salt Lake City, UT, USA.

He worked as a Research Assistant during his masters in Michigan Technological University and currently he is working as a Research Assistant at the University of Utah, Salt Lake City, UT. In summer 2018, he worked as a PV Electrical Characterization Intern in National Renewable Energy Laboratory (NREL). His current research interests include reliability, testing, manufacturing, measurements, and characterization of photovoltaic systems.



Evan J. Benoit received a B.S. degree in Nuclear Engineering Technology from Excelsior College in 2015. He received his B.S. and M.S. degrees in Electrical Engineering from the University of Utah in 2019. He is currently pursuing a Ph.D. in Electrical Engineering at the University of Utah.

From 2005 to 2015, he was a Submarine Nuclear Field Electrician's Mate in the US Navy. He began working as a Research Assistant at the University of Utah, Salt Lake City UT during the summer of 2018. His research explores the applicability of spread spectrum time domain reflectometry for identification of complex impedances on transmission lines. Benoit is a member of the Golden Key International Honour Society, the National Society of Leadership and Success, and a student member of IEEE.



Ayobami S. Edun received the B.Eng. degree in Electrical and Electronics Engineering from Federal University of Technology, Akure, Nigeria in 2014. He received the M.S. degree in Electrical and Computer Engineering from University of Florida, Gainesville, FL, USA in 2019. He is currently working towards the Ph.D. degree in Electrical and Computer Engineering at the University of Florida, Gainesville, FL, USA. He currently works as a Research Assistant at the SmartDATA Lab, University of Florida, Gainesville, FL. He has been working with spread spectrum time domain reflectometry (SSTDR) in being able to detect, localize, and characterize faults within solar panel system.



Cynthia M. Furse (M'85–SM'99–F'08) is Professor of Electrical and Computer Engineering at the University of Utah. Furse received her B.S. in Electrical Engineering with a Mathematics minor in 1985, M.S. degree in Electrical Engineering in 1988, and her Ph.D. in Electrical Engineering from the University of Utah in 1994.

She has applied her expertise in electromagnetics to sensing and communication in complex lossy scattering media such as the human body, geophysical prospecting, ionospheric plasma, and aircraft wiring networks. She has taught electromagnetics, wireless communication, computational electromagnetics, microwave engineering, antenna design, and introductory electrical engineering and has been a leader in the development of the flipped classroom.

Furse is a Fellow of the IEEE and the National Academy of Inventors. She is a past AdCom member for the IEEE AP Society and past chair of the IEEE AP Education Committee. She has received numerous teaching and research awards including the 2020 IEEE Chen To Tai Distinguished Educator Award. She is a founder of LiveWire Innovation, Inc., a spin-off company commercializing devices to locate intermittent faults on live wires.



Michael A. Scarpulla (M'05-SM'14) earned the Sc.B. degree from Brown University in 2000 and the Ph.D. from UC Berkeley in 2006, both in Materials Science and Engineering. His Ph.D. work focused on laser processing of ion implanted compound semiconductors, carrier mediated ferromagnetism, and multiband semiconductors.

From 2006-2008 he was a Postdoctoral Scholar at UC Santa Barbara working on epitaxial integration of rare-earth pnictides with III-V semiconductors using MBE. Since joining the ECE and MSE faculties at University of Utah in 2008, he has worked in light trapping for photovoltaics, materials processing and characterization of chalcogenide thin film photovoltaics, reflectometry in photovoltaic systems, and defects in wide-bandgap semiconductors. His hobbies include skiing, climbing, and other mountain adventures.



Joel B. Harley (S'05-M'14) received his B.S. degree in Electrical Engineering from Tufts University in Medford, MA, USA. He received his M.S. and Ph.D. degrees in Electrical and Computer Engineering from Carnegie Mellon University in Pittsburgh, PA, USA in 2011 and

2014, respectively.

In 2018, he joined the University of Florida, where he is currently an Assistant Professor in the Department of Electrical and Computer Engineering. Previously, he was an Assistant Professor in the Department of Electrical and Computer Engineering at the University of Utah. His research interests include integrating novel signal processing, machine learning, and data science methods for the analysis of waves and time-series data.

Harley's awards and honors include 2020 IEEE Ultrasonics, Ferroelectrics, and Frequency Control Society Star Ambassador Award, a 2020 and 2018 Air Force Summer Faculty Fellowship, a 2017 Air Force Young Investigator Award, a 2014 Carnegie Mellon A. G. Jordan Award (for academic excellence and exceptional service to the community). He has published more than 90 technical journal and conference papers, including four best student papers. He is a student representative advisor for the IEEE Ultrasonics, Ferroelectrics, and Frequency Control Society, a member of the IEEE Signal Processing Society, and a member of the Acoustical Society of America.